

# AutoNeRF: Training Implicit Scene Representations with Autonomous Agents

Pierre Marza<sup>1\*</sup> Laetitia Matignon<sup>2</sup> Olivier Simonin<sup>1</sup> Dhruv Batra<sup>3,5</sup>  
 Christian Wolf<sup>4</sup> Devendra Singh Chaplot<sup>3</sup>  
<sup>1</sup>INSA Lyon <sup>2</sup>UCBL <sup>3</sup>Meta AI <sup>4</sup>Naver Labs Europe <sup>5</sup>Georgia Tech  
 Project Page: <https://pierre.marza.github.io/projects/autonerf/>

## Abstract

Implicit representations such as Neural Radiance Fields (NeRF) have been shown to be very effective at novel view synthesis. However, these models typically require manual and careful human data collection for training. In this paper, we present AutoNeRF, a method to collect data required to train NeRFs using autonomous embodied agents. Our method allows an agent to explore an unseen environment efficiently and use the experience to build an implicit map representation autonomously. We compare the impact of different exploration strategies including hand-crafted frontier-based exploration, end-to-end and modular approaches composed of trained high-level planners and classical low-level path followers. We train these models with different reward functions tailored to this problem and evaluate the quality of the learned representations on four different downstream tasks: classical viewpoint rendering, map reconstruction, planning, and pose refinement. Empirical results show that NeRFs can be trained on actively collected data using just a single episode of experience in an unseen environment, and can be used for several downstream robotic tasks, and that modular trained exploration models outperform other classical and end-to-end baselines. Finally, we show that AutoNeRF can reconstruct large-scale scenes, and is thus a useful tool to perform scene-specific adaptation as the produced 3D environment models can be loaded into a simulator to fine-tune a policy of interest.

## 1. Introduction

Exploration is a key challenge in building autonomous navigation agents that operate in unseen environments. In the last few years, there has been a significant amount of work on training exploration policies to maximize coverage [6, 9, 38], find goals specified by object categories [17,

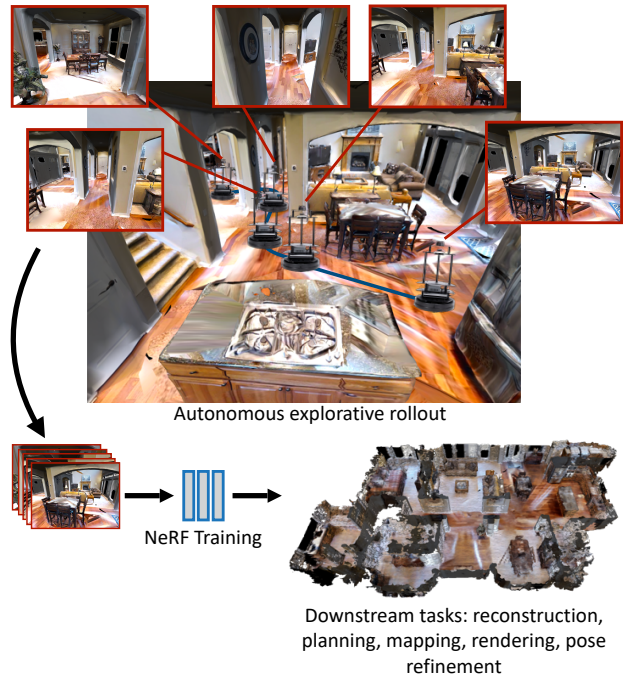


**Figure 1:** We propose a method for automatically generating 3D models of a scene by training NeRFs from data collected by autonomous agents. We compare classical and RL-trained exploration policies, with different reward definitions and evaluate the implicit representations on reconstruction, planning, mapping, rendering, and pose refinement.

5, 26, 35, 37], images [58, 8, 18, 29] or language [3, 21, 31] and for embodied active learning [7, 4]. Among these methods, modular learning methods have shown to be very effective at various embodied tasks [6, 5, 11, 15]. These methods learn an exploration policy that can build an explicit semantic map of the environment which is then used for planning and downstream embodied AI tasks such as Object Goal or Image Goal Navigation.

Concurrently, in the computer graphics and vision communities, there has been a recent but large body of work on learning implicit map representations, particularly based

\*Work done during an internship at Meta AI  
 Correspondence: [pierre.marza@insa-lyon.fr](mailto:pierre.marza@insa-lyon.fr)

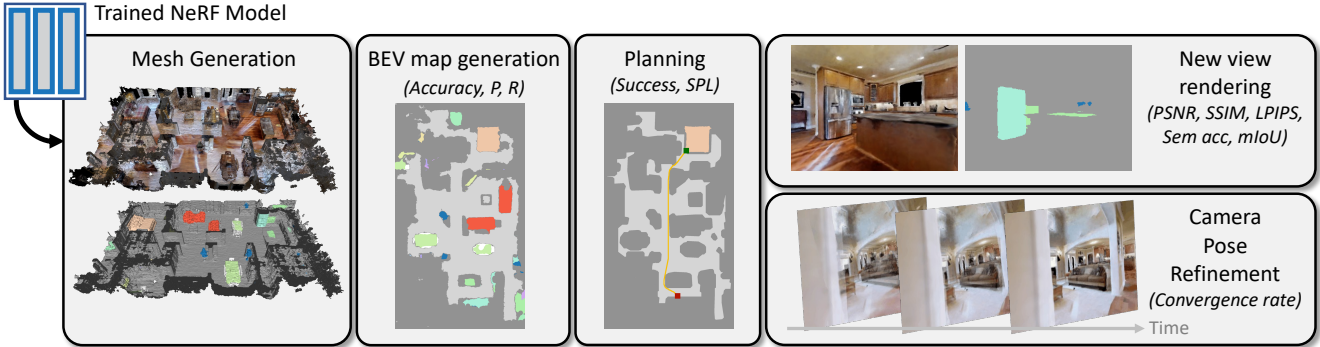


**Figure 2: Downstream tasks** — the model trained from autonomously collected data is used for several downstream tasks related to robotics: Mesh generation for the covered scene (color or semantic mesh); Birds-eye-view map generation and navigation/planning on this map; new view generation of RGB and semantic frames; camera pose refinement (visual servoing).

on Neural Radiance Fields (NeRF) [30, 32, 14, 53, 49]. Prior methods [45, 47, 56, 57] demonstrate strong performance in novel view synthesis and are appealing from a scene understanding point of view as a compact and continuous representation of appearance and semantics in a 3D scene. However, most approaches building implicit representations require data collected by humans [30, 45, 57]. Can we train embodied agents to explore an unseen environment efficiently to collect data that can be used to create implicit map representations or NeRFs autonomously? In this paper, our objective is to tackle this problem of active exploration for autonomous NeRF construction. If an embodied agent is able to build an implicit map representation autonomously, it can then use it for a variety of downstream tasks such as planning, pose estimation, and navigation. Just a single episode or a few minutes of exploration in an unseen environment can be sufficient to build an implicit representation that can be utilized for improving the performance of the agent in that environment for several tasks without any additional supervision.

In this work, we introduce AutoNeRF, a modular policy trained with Reinforcement Learning (RL) that can explore an unseen 3D scene to collect data for training a NeRF model autonomously (Figure 1). While most prior work evaluates NeRFs on rendering quality, we propose a range of downstream tasks to evaluate them (and indirectly, the exploration policies used to gather data for training these representations) for Embodied AI applications. Specifically, we use geometric and semantic map prediction accuracy, planning accuracy for Object Goal and Point Goal navigation and camera pose refinement (Figure 2). We show that AutoNeRF outperforms the well-known frontier-based exploration algorithm as well as state-of-the-art end-to-end learnt policies, and also study the impact of different reward functions on the downstream performance of the NeRF model. We also study how AutoNeRF can be used as a tool to autonomously adapt policies to a specific scene at deployment time by providing a high-quality reconstruction

of large-scale environments that can be loaded into a simulator to improve the performance of any given agent safely.

## 2. Related Work

**Neural fields** — represent the structure of a 3D scene with a neural network. They were initially introduced in [28, 34, 10] as an alternative to discrete representations such as voxels [27], point clouds [13] or meshes [16]. Neural Radiance Fields (NeRF) [30] then introduced a differentiable volume rendering loss allowing to supervise 3D scene reconstruction from 2D supervision, achieving state-of-the-art performance on novel view synthesis. Follow-up work has addressed faster training and inference [32, 14], or training from few images [53]. A recent survey [49] references different advances in this growing field.

**Neural fields in robotics** — implicit representations are not limited to novel view synthesis, they have also been proposed for real-time SLAM [43, 60, 59]. Initial work [43] required RGB-D input and was deployed on limited-size environments. [60] introduced a hierarchical implicit representation to represent larger scenes, and [59] now only requires RGB input. Extensions incorporate semantics: [43] augmented NERFs with a semantic head [56] trained from sparse and noisy 2D semantic maps. Implicit representations have also been used to represent occupancy, explored area, and semantic objects to navigate towards [25], or as a representation of the density of a scene for drone obstacle avoidance [1]. They have been used for camera pose refinement through SGD directly on a loss in rendered pixel space [52]. In contrast to the literature, we investigate training these representations from data collected by autonomous agents directly and explore the effect of the choice of policy on downstream robotics tasks.

**Active learning for neural fields** — has not yet been extensively studied. Most work focuses on fixed datasets of 2D frames, work studies the active selection of training

data. ActiveNeRF [33] estimates the uncertainty of a NeRF model by expressing radiance values as Gaussian distributions. ActiveRMAP [54] minimizes collisions and maximizes an entropy-based information gain metric. All these methods target very small scenes in non-robotic scenarios, either single objects or forward-facing only. In contrast, we start from unknown environments and actively explore large indoor scenes requiring robotic exploration policies capable of handling complex scene understanding and navigation.

**Autonomous scene exploration** — visual navigation and exploration are well-studied topics in robotics. It is generally defined as a coverage maximization problem, a well-known baseline being Frontier-Based Exploration (FBE) [51]. Different variants exist [12, 20, 50] but the core principle is to maintain a frontier between explored and unexplored space and to sample points on the frontier. Several learning-based exploration approaches are also explored in recent work [6, 9, 38]. In our case, we target scene exploration with a different goal than maximizing vanilla coverage: we study how different definitions of exploration impact the quality of an implicit scene representation.

### 3. Background

To make the paper self-contained, we first briefly recall relevant background on modular exploration policies, and neural radiance fields.

#### 3.1. Modular exploration policies

The trained policy aims to allow an agent to explore a 3D scene to collect a sequence of 2D RGB and semantic frames and camera poses, that will be used to train the continuous scene representation. Following [5, 6], we adapt a modular policy composed of a *Mapping* process that builds a *Semantic Map*, a *Global Policy* that outputs a global waypoint from the semantic map as input, and finally, a *Local Policy* that navigates towards the global goal, see Figure 3.

**Semantic Map** — a 2D top-down map is maintained at each time step  $t$ , with several components: (i) an occupancy component  $\mathbf{m}_t^{occ} \in \mathbb{R}^{M \times M}$  stores information on free navigable space; (ii) an exploration component  $\mathbf{m}_t^{exp} \in \mathbb{R}^{M \times M}$  sets to 1 all cells which have been within the agent’s field of view since the beginning of the episode; (iii) a semantic component  $\mathbf{m}_t^{sem} \in \mathbb{R}^{S \times M \times M}$ , where  $M \times M$  is the spatial size and  $S$  denotes the number of channels storing information about the scene. Additional maps store the current and previous agent locations. All maps are updated at each timestep from sensor information. Structural components are updated by inverse projection of the current depth observation and pooling to the ground plane, a similar computation is done for the exploration component. The semantic maps additionally use predictions obtained with Mask R-CNN [19]. Egocentric maps are integrated over time taking

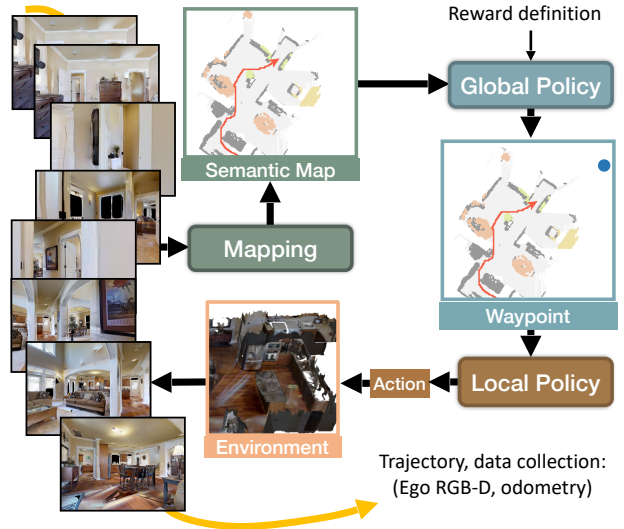


**Figure 3:** We adapted the modular policy in [5]: a mapping module generates a semantic and occupancy top-down map from ego-centric RGB-D observations and sensor pose. A high-level policy trained with RL predicts global waypoints, which are followed by a handcrafted low-level policy (fast marching). The sequence of observations comprises the data input to NeRF training.

into account agent poses estimated from sensor information.

**Policies** — intermediate waypoints are predicted by the *Global Policy*, a convolutional neural network taking as input the stacked maps (we use the architecture in [5]) and is trained with RL/PPO [40]. A *Local Policy* navigates towards the waypoint taking discrete actions for 25 steps with the analytical *Fast Marching Method* [41].

#### 3.2. Neural radiance fields

**Vanilla Semantic NeRF** — Neural Radiance Fields [30] are composed of MLPs predicting the density  $\sigma$ , color  $c$  and, eventually as in [56], the semantic class  $s$  of a particular 3D position in space  $\mathbf{x} \in \mathbb{R}^3$ , given a 2D camera viewing direction  $\phi \in \mathbb{R}^2$ . NeRFs have been designed to render new views of a scene provided a camera position and viewing direction. The color of a pixel is computed by performing an approximation of volumetric rendering, sampling  $N$  quadrature points along the ray. Given multiple images of a scene along with associated camera poses, a NeRF is trained with Stochastic Gradient Descent minimizing the difference between rendered and ground-truth images.

**Enhanced NeRF (Semantic Nerfacto)** — we leverage recent advances to train NeRF models faster while maintaining high rendering quality and follow what is done in the Nerfacto model from [46], that we augment with a semantic head. The inputs  $\mathbf{x}$  and  $\phi$  are augmented with a learned appearance embedding  $\mathbf{e} \in \mathbb{R}^{32}$ . Both  $\mathbf{x}$  and  $\phi$  are first encoded using respectively a hash encoding function  $h$  as

$\tilde{\mathbf{x}} = h(\mathbf{x})$  and a spherical harmonics encoding function  $sh$  as  $\tilde{\phi} = sh(\phi)$ .  $\tilde{\mathbf{x}}$  is fed to an MLP  $f_d$  predicting the density at the given 3D position, yielding  $(\sigma, \mathbf{h}_d) = f_d(\tilde{\mathbf{x}}; \Theta_d)$ , where  $\mathbf{h}_d$  is a latent representation.  $\mathbf{h}_d$  is fed to another MLP model  $f_s$  that outputs a softmax distribution over the  $S$  considered semantic classes as  $\mathbf{s} = f_s(\mathbf{h}_d; \Theta_s)$  where  $\mathbf{s} \in \mathbb{R}^S$ . Finally,  $\mathbf{h}_d$ ,  $\tilde{\phi}$  and  $\mathbf{e}$  are the inputs to  $f_c$  that predicts the RGB value at the given 3D location,  $\mathbf{c} = f_c(\mathbf{h}_d, \tilde{\phi}, \mathbf{e}; \Theta_c)$  where  $\mathbf{c} \in \mathbb{R}^3$ .

At training time, points must be sampled along shot rays to reconstruct image pixels. First, piecewise sampling will choose half of the points uniformly up to a distance  $d_s$  from the camera, the other half of the points are distributed with an increasing step size. In the second step, this initial set of samples is improved by proposal sampling, which consolidates samples in regions that have the most impact on the final rendering. This requires a fast query and coarse density representation, different from the neural field itself, implemented as a small MLP with hash encoding.

## 4. AutoNeRF

We present AutoNeRF, a method to collect data required to train NeRFs using autonomous embodied agents. In our task setup, the agent is initialized in an unseen environment and is tasked with gathering data in a single episode with a fixed time budget. The observations collected by the agent in this single trajectory are used to train a neural implicit representation of the scene, which will serve as a compact and continuous representation of the density, the RGB appearance, and the semantics of the considered scene. Finally, the trained scene model is evaluated on several downstream tasks in robotics: new view rendering, mapping, planning and pose refinement.

**Task Specification** — The agent is initialized at a random location in an unknown scene and at each timestep  $t$  can execute discrete actions in the space  $\Lambda = \{\text{FORWARD } 25\text{cm}, \text{TURN\_LEFT}, \text{TURN\_RIGHT}\}$ . At each step, the agent receives an observation  $\mathbf{o}_t$  composed of an egocentric RGB frame and a depth map. The field of view of the agent is  $90^\circ$ . It also has access to odometry information. The agent can navigate for a limited number of 1500 discrete steps.

AutoNeRF can be broken down into two phases: Exploration Policy Training and NeRF Training. In the first phase, we train an exploration policy to collect the observations. The policy is self-supervised, it is trained in a set of training environments using intrinsic rewards. In the second phase, we use the trained exploration policy to collect data in unseen test scenes, one trajectory per scene, and train a NeRF model using this data. The trained NeRF model is then evaluated on the set of downstream tasks.

## 4.1. Exploration Policy Training

As described in Section 3.1, we use a modular exploration policy architecture with the Global Policy primarily responsible for exploration. We consider different reward signals for training the Global Policy tailored to our task of scene reconstruction, and which differ in the importance they give to different aspects of the scene. All these signals are computed in a self-supervised fashion using the metric map representations built by the exploration policy.

**Explored area** — (*Ours (cov.)*) optimizes the coverage of the scene, i.e. the size of the explored area, and has been proposed in the literature, e.g. in [5, 6]. It accumulates differences in the exploration component  $\mathbf{m}_t^{exp}$ ,

$$r_t^{cov} = \sum_{i=0}^{M-1} \sum_{j=0}^{M-1} \mathbf{m}_t^{exp}[i, j] - \mathbf{m}_{t-1}^{exp}[i, j]$$

**Obstacle coverage** — (*Ours (obs.)*) optimizes the coverage of obstacles in the scene, and accumulates differences in the corresponding component  $\mathbf{m}_t^{occ}[i, j]$ . It targets tasks where obstacles are considered more important than navigable floor space, which is arguably the case when viewing is less important than navigating.

$$r_t^{obs} = \sum_{i=0}^{M-1} \sum_{j=0}^{M-1} \mathbf{m}_t^{occ}[i, j] - \mathbf{m}_{t-1}^{occ}[i, j]$$

**Semantic object coverage** — (*Ours (sem.)*) optimizes the coverage of the  $S$  semantic classes detected and segmented in the semantic metric map  $\mathbf{m}_t^{sem}$ . This reward removes obstacles that are not explicitly identified as a notable semantic class — see section 5 for their definition.

$$r_t^{sem} = \sum_{i=0}^{M-1} \sum_{j=0}^{M-1} \sum_{k=0}^{S-1} \mathbf{m}_t^{sem}[i, j, k] - \mathbf{m}_{t-1}^{sem}[i, j, k]$$

**Viewpoints coverage** — (*Ours (view.)*) optimizes for the usage of the trained implicit representation as a dense and continuous representation of the scene usable to render arbitrary new viewpoints, either for later visualization as its own downstream task or for training new agents in simulation. To this end, we propose to maximize coverage not only in terms of agent positions but also in terms of agent viewpoints. Compared to [5], we introduce an additional 3D map  $\mathbf{m}_t^{view}[i, j, k]$ , where the first two dimensions correspond to spatial 2D positions in the scene and the third dimension corresponds to a floor plane angle of the given cell discretized into  $V=12$  bins. A value of  $\mathbf{m}_t^{view}[i, j, k] = 1$  indicates that cell  $(i, j)$  has been seen by the agent from a (discretized) angle  $k$ . The reward maximizes its changes,

$$r_t^{view} = \sum_{i=0}^{M-1} \sum_{j=0}^{M-1} \sum_{k=0}^{V-1} \mathbf{m}_t^{view}[i, j, k] - \mathbf{m}_{t-1}^{view}[i, j, k]$$

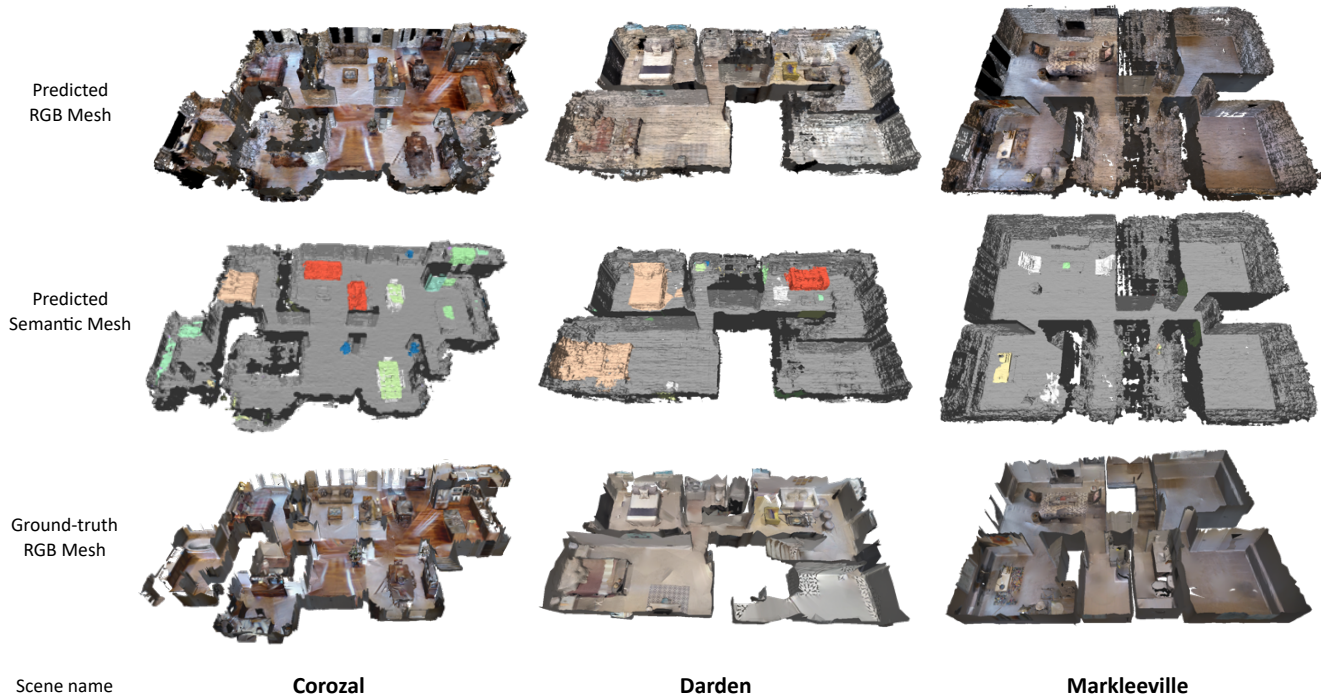


**Figure 4: Mesh reconstruction:** reconstruction of 3 Gibson val scenes extracted from a NeRF model trained on data gathered by our modular policy. Both geometry, semantics, and appearance are satisfying. Exploration with the modular policy, *Ours (obs)*.

## 4.2. NeRF training

The sequence of observations collected by the agent comprises egocentric RGB frames  $\{\mathbf{o}_t\}_{t=1\dots T}$ , first-person semantic segmentations  $\{\mathbf{s}_t\}_{t=1\dots T}$  and associated poses  $\{\mathbf{p}_t\}_{t=1\dots T}$  in a reference frame, which we define as the starting position  $t=0$  of each episode. In our experiments, we leverage privileged pose and semantics information from simulation. We also conduct an experiment showcasing the difference between using GT semantics from a simulator and a Mask R-CNN [19] model. As in [56], we add a semantic head to the implicit representation, which predicts the semantic classes defined in the segmentation maps  $\{\mathbf{s}_t\}$  given the internal latent representation calculated for each pixel.

An important property of this procedure is that no depth information is required for reconstruction. The implicit representation is trained by mapping pixel coordinates  $\mathbf{x}_i$  for each pixel  $i$  to RGB values and semantic values with the volume rendering loss described in Section 3.2. The input coordinates  $\mathbf{x}_i$  are obtained using the global poses  $\mathbf{p}_t$  and intrinsics from calibrated cameras.

## 4.3. Downstream tasks

Prior work on implicit representations generally focused on two different settings: (i) evaluating the quality of a neural field based on its new view rendering abilities given a dataset of (carefully selected) training views, and (ii) evalu-

ating the quality of a scene representation in robotics conditioned on given (constant) trajectories, evaluated as reconstruction accuracy. We cast this task in a more holistic way and more aligned with our scene understanding objective. We evaluate the impact of trajectory generation (through exploration policies) directly on the quality of the representation, which we evaluate in a goal-oriented way through multiple tasks related to robotics (cf. Figure 2).

**Task 1: Rendering** — This task is the closest to the evaluation methodology prevalent in the neural field literature. We evaluate the rendering of RGB frames and semantic segmentation as proposed in [56]. Unlike the common method of evaluating an implicit representation on a subset of frames within the trajectory, we evaluate it on a set of uniformly sampled camera poses within the scene, independently of the trajectory taken by the policy. This allows us to evaluate the representation of the complete scene and not just its interpolation ability.

We render ground-truth images and semantic masks associated with sampled camera poses using the Habitat [39, 44] simulator and compare them against the NeRF rendering. RGB rendering metrics are PSNR (*Peak Signal-to-Noise Ratio*), SSIM (*Structural Similarity Index Measure*) and LPIPS [55]. PSNR estimates absolute errors while SSIM evaluates the amount of retrieved structural information in the image by incorporating priors such as pixel interdependencies, and LPIPS attempts to reflect human per-



**Figure 5: Rollouts by Frontier-Based Exploration vs. Modular policy (obs cov):** FBE properly covers the scene, but does not collect a large diversity of viewpoints, while the modular policy enters the rooms and thus provides richer training data for the neural field.

ception by computing distance between GT and rendered frames in the feature space of a VGG network [42]. Rendering of semantics is evaluated in terms of avg. per-class accuracy and mean intersection over union (mIoU).

**Task 2: Metric Map Estimation** — While rendering quality is linked to perception of the scene, it is not necessarily a good indicator of its structural content, which is crucial for robotic downstream tasks. We evaluate the quality of the estimated structure by translating the continuous representation into a format, which is very widely used in map-and-plan baselines for navigation, a binary top-down (bird’s-eye-view=BEV) map storing occupancy and semantic category information and compare it with the ground-truth from the simulator. We evaluate obstacle and semantic maps using accuracy, precision, and recall.

**Task 3: Planning** — Using maps for navigation, it is difficult to pinpoint the exact precision required for successful planning, as certain artifacts and noises might not have a strong impact on reconstruction metrics, but could lead to navigation problems, and vice-versa. We perform goal-oriented evaluation and measure to what extent path planning can be done on the obtained top-down maps.

We sample 100 points on each scene and plan from those starting points to two different types of goals: to selected end positions, *PointGoal* planning, and to objects categories, *ObjectGoal* planning. The latter, *ObjectGoal*, requires planning the shortest path from the given starting point to the closest object of each semantic class available on the given scene. For both tasks, we plan with the *Fast Marching Method* and report both mean *Success* and *SPL* as introduced in [2]. For a given episode, *Success* is 1 if planning stops < 1m from the goal and *SPL* measures path efficiency.

**Task 4: Pose Refinement** — This task [52] involves correcting an initial noisy camera position and associated ren-

dered view and optimizing the position until a given ground-truth position is reached, which is given through its associated rendered view only. The optimization process therefore leads to a trajectory in camera pose space. This task is closely linked to visual servoing with a “eye-in-hand” configuration, a standard problem in robotics, in particular in its “direct” variant [24], where the optimization is directly performed over losses on the observed pixel space.

We address this problem by taking the trained NeRF model  $f$  and freezing its weights  $\theta$ . In what follows, we will denote the function rendering a full image  $\mathbf{o}$  given camera pose  $c$  and viewing direction  $\phi$  as  $\mathbf{o} = \mathcal{R}(c, \phi)$ . Then, given a ground truth view  $\mathbf{o}^*$ , the camera position and direction can be directly optimized from a starting position  $(c, \phi)^{[0]}$  with gradient descent as

$$(c, \phi)^{[t+1]} = (c, \phi)^{[t]} + \nu \left[ \frac{\partial \mathcal{L}(\mathbf{o}^*, \mathcal{R}(c, \phi))}{\partial c, \phi} \right],$$

where  $\mathcal{L}$  is the MSE (Mean Squared Error) loss and  $\nu$  is a learning rate.

To generate episodes of starting and end positions, we take 100 sampled camera poses in each scene and apply a random transformation to generate noisy poses. The model is evaluated in terms of rotation and translation convergence rate, i.e. percentage of samples where the final difference with ground truth is less than  $3^\circ$  in rotation and  $2cm$  in translation. We also report the mean translation and rotation errors for the converged samples.

## 5. Experimental Results

**Modular Policy training** — is performed on one V100 GPU for 7 days. All modular policies are trained on the 25 scenes of the Gibson [48]-tiny training set. The used Mask R-CNN model is pre-trained on the MS COCO dataset [22] and finetuned on Gibson train scenes. We consider  $S=15$  semantic categories:  $\{chair, couch, potted\ plant, bed, toi-$

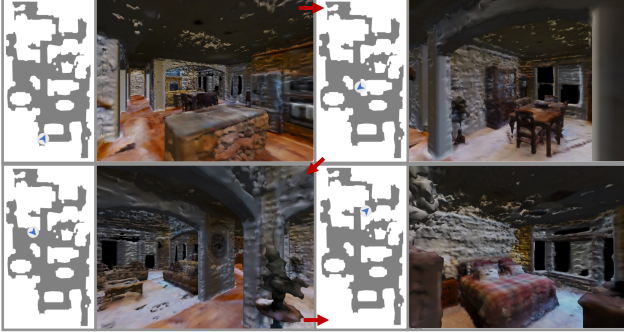


**Figure 6: Navigating in the Habitat simulator:** the underlying mesh was extracted from the trained NeRF, *Ours (cov)*. Rendering quality and the generated BEV map are correct, as are free navigable space and collision handling. Temporal order indicated by  $\rightarrow$ .

*let, tv, dining table, oven, sink, refrigerator, book, clock, vase, cup, bottle* }.

**External baselines** — We compare our trained modular policies against the classical Frontier-Based Exploration algorithm (*Frontier*), as well as end-to-end policies trained with RL. More specifically, we consider 4 end-to-end policies from [36], that all share the same architecture but were trained with different exploration-related reward functions: coverage (*E2E (cov.)*), curiosity (*E2E (cur.)*), novelty (*E2E (nov.)*), reconstruction (*E2E (rec.)*). Reward functions are presented in [36].

**Evaluation** — consists in running 5 rollouts with different start positions in each of the 5 Gibson-tiny val scenes for each policy, always on the first house floor. A NeRF model is then trained on each trajectory data.

**NeRF models** — In our experiments, we consider two different NeRF variants presented in Section 3.2. Most experiments are conducted with *Semantic Nerfacto*, as it provides a great trade-off between training speed and quality of representation. *Semantic Nerfacto* is built on top of the *Nerfacto* model from the nerfstudio [46] library. We augment the model with a semantic head and implement evaluation on test camera poses independently from the collected trajectory. Only the next two subsections (5.1, 5.2) will involve training a *vanilla Semantic NeRF* model, more precisely the one introduced in [56] that also contains a semantic head. We chose this variant for these specific experiments to illustrate the possibility of providing high-fidelity representations of complex scenes, and show that a *vanilla Semantic NeRF* model trained for a longer time (12h) leads to better-estimated geometry. Results from *Semantic Nerfacto* are still very good (see Figures 7 and 8) but we found meshes to be of higher quality with a vanilla NeRF model.

Policy	Success $\uparrow$	SPL $\uparrow$
<i>Finetuned on Gibson meshes (not comparable)</i> <sup>†</sup>	99.7	97.9
<b>Pre-trained (no finetuning)</b>	90.2	82.9
<b>Finetuned on AutoNeRF meshes</b>	<b>92.9</b>	<b>86.7</b>

**Table 1: PointGoal Finetuning:** finetuning a PointGoal agent on a mesh automatically collected from a rollout and a NeRF with AutoNeRF improves mean performance over a pre-trained policy on a specific scene. <sup>†</sup> an upper bound which finetunes on the original mesh. In a real use case involving a robot automatically collecting data, this mesh would not be available (not comparable).

Policy	RGB			Semantics	
	PSNR $\uparrow$	SSIM $\uparrow$	LPIPS $\downarrow$	Per-class acc $\uparrow$	mIoU $\uparrow$
<b>Frontier</b>	19.75	0.743	0.343	81.4	65.7
<b>E2E (cov.)</b>	20.94	0.750	0.332	80.1	63.9
<b>E2E (cur.)</b>	20.60	0.747	0.338	78.7	61.9
<b>E2E (nov.)</b>	23.36	0.801	0.268	84.6	71.4
<b>E2E (rec.)</b>	23.17	0.797	0.270	84.1	70.5
<b>Ours (cov.)</b>	24.89	0.837	0.218	90.2	81.2
<b>Ours (sem.)</b>	25.34	0.843	0.207	<b>91.9</b>	81.8
<b>Ours (obs.)</b>	<b>25.56</b>	<b>0.846</b>	<b>0.203</b>	<b>91.8</b>	<b>83.2</b>
<b>Ours (view.)</b>	25.17	0.842	0.211	91.3	82.0

**Table 2: Rendering performance** on uniformed sampled viewpoints of the full scene after training on a single trajectory.

Policy	Occupancy			Semantics		
	Acc. $\uparrow$	Prec. $\uparrow$	Rec. $\uparrow$	Acc. $\uparrow$	Prec. $\uparrow$	Rec. $\uparrow$
<b>Frontier</b>	81.2	86.9	49.9	99.7	26.6	21.0
<b>E2E (cov.)</b>	77.1	86.2	50.4	99.7	22.1	16.1
<b>E2E (cur.)</b>	81.8	90.3	50.7	99.7	19.2	12.5
<b>E2E (nov.)</b>	83.1	88.7	61.3	99.7	25.5	18.3
<b>E2E (rec.)</b>	81.6	87.6	60.0	99.7	26.2	18.0
<b>Ours (cov.)</b>	86.8	89.1	74.7	99.8	35.1	27.1
<b>Ours (sem.)</b>	86.6	88.3	76.5	99.8	35.7	29.8
<b>Ours (obs.)</b>	86.4	89.4	76.5	99.8	36.2	29.8
<b>Ours (view.)</b>	<b>88.1</b>	<b>90.9</b>	<b>77.0</b>	99.8	<b>37.4</b>	<b>30.2</b>

**Table 3: Map estimation performance:** comparison of BEV maps estimated from the NeRF.

## 5.1. Reconstructing house-scale scenes

We illustrate the possibility of autonomously reconstructing complex large-scale environments such as apartments or houses from the continuous representations trained on data collected by agents exploring the scene using the modular policy. Figure 4 shows RGB and semantic meshes for 3 Gibson val scenes. Geometry, appearance, and semantics are satisfying. In Figure 6 we show that such meshes can be loaded into the Habitat simulator and allow proper navigation and collision computations. Both occupancy top-down map generation and RGB renderings are performed by the Habitat simulator from the generated mesh.

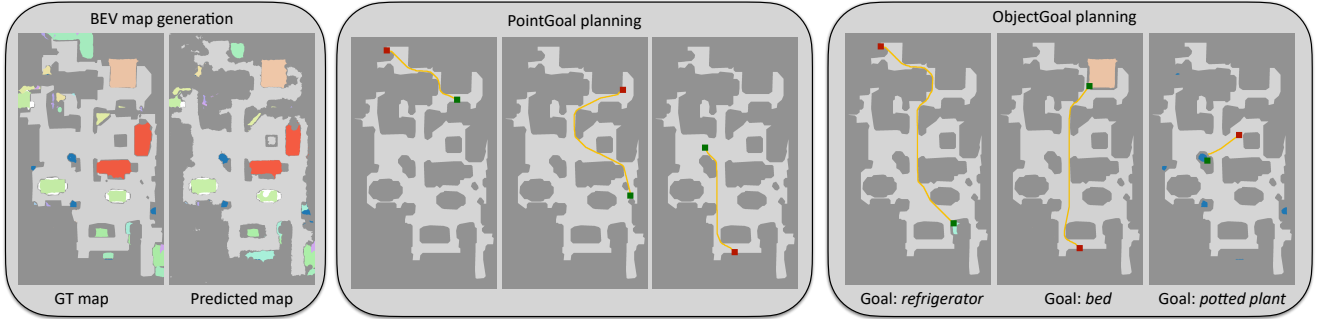


Figure 7: BEV map tasks: Generation of semantic BEV maps (Left), *PointGoal* (Middle) and *ObjectGoal* planning (Right).

## 5.2. Autonomous adaptation to a new scene

The long-term goal of Embodied AI is to train general policies that can be deployed on any new scene and perform a task of interest. Even if some policies already showcase strong generalization abilities, they will likely struggle with some specificities of a given environment. When considering the deployment of trained agents on real robots in a house or apartment, such failure modes can be problematic. A scene-specific adaptation of a pre-trained policy thus appears as a relevant alternative to learn about a new environment. However, such adaptation should happen in simulation to ensure safety. We here explore the usage of AutoNeRF to first explore the environment to build a 3D representation, which is then loaded into a simulator to safely finetune a policy of interest. More specifically, we consider a policy for an agent taking a depth frame as input at each timestep  $t$  and pre-train it on *PointGoal* navigation on the Gibson train scenes. It is then fine-tuned on 4 Gibson val scenes, using meshes generated with AutoNeRF, before being evaluated on the original Gibson meshes. Sampling of training and validation episodes, as well as training and validation, are performed in the Habitat simulator. For each environment, we sample  $50k$  episodes from our mesh to finetune the policy for  $10M$  training frames using PPO with a learning rate of  $2.5e-6$ . For evaluation, we sample  $1k$  episodes per scene on the original Gibson meshes and report mean Success and SPL. Table 1 shows that the pre-trained policy already achieves great performance. However, some validation episodes fail because of certain specific scene configurations. Scene-specific finetuning on autonomously reconstructed 3D meshes allows to improve both Success and SPL compared with the pre-trained policy.

We also compare with finetuning directly on the Gibson mesh (for  $10M$  frames with a learning rate of  $2.5e-5$ ), which provides a non-comparable soft upper bound — in a real robotics scenario, these meshes would not be accessible. We can see that performance could still be improved further by increasing mesh reconstruction quality. However, it is important to note that the mistakes from the pre-trained

Policy	PointGoal		ObjectGoal	
	Succ. $\uparrow$	SPL $\uparrow$	Succ. $\uparrow$	SPL $\uparrow$
<b>Frontier</b>	22.4	21.4	9.6	9.1
<b>E2E (cov.)</b>	30.0	29.3	8.9	8.3
<b>E2E (cur.)</b>	29.8	29.2	8.5	8.0
<b>E2E (nov.)</b>	32.3	31.9	11.4	10.8
<b>E2E (rec.)</b>	32.8	32.6	10.5	10.0
<b>Ours (cov.)</b>	<b>39.5</b>	<b>39.0</b>	14.8	14.3
<b>Ours (sem.)</b>	37.7	37.4	<b>16.0</b>	<b>15.4</b>
<b>Ours (obs.)</b>	38.2	37.8	<b>15.8</b>	<b>15.3</b>
<b>Ours (view.)</b>	39.0	38.6	<b>15.9</b>	<b>15.3</b>

Table 4: Planning performance on the BEV maps estimated from the NeRF obtained with the *Fast Marching* method.

policy occur in very specific places in the environment, and thus reaching the performance of the upper bound might be about reconstructing fine details.

## 5.3. Quantitative results

**Frontier-Based Exploration vs Modular Policy** — as can be seen from the quantitative comparisons on the different downstream tasks (Tables 2, 3, 4, 5), RL-trained modular policies outperform FBE on all metrics and should thus be considered as the preferred means of collecting NeRF data. This is a somewhat surprising result, since Frontier-Based Exploration generally performs satisfying visual coverage of the scene, even though it can sometimes get stuck because of map inaccuracies. This shows that vanilla visual coverage, the optimized metrics in many exploration-oriented tasks, is not a sufficient criterion to collect data for NeRF training. Figure 5 illustrates this point with rollouts from FBE and a modular policy trained to maximize obstacle coverage. FBE properly covers the scene but does not necessarily cover a large diversity of viewpoints, while the modular policy provides richer training data to the NeRF.

**End-to-end Policy vs Modular Policy** — Tables 2, 3, 4, 5 also show that the modular policies outperform end-to-end RL policies on all considered metrics. Interestingly, *novelty* and *reconstruction* seem to be the best reward functions from [36] when training end-to-end policies if the final goal



Policy	Conv. rate $\uparrow$	Rot. Error ( $^\circ$ ) $\downarrow$	Trans. Error (m) $\downarrow$
<b>Frontier</b>	7.2	0.383	0.00955
<b>E2E (cov.)</b>	15.4	0.319	0.00775
<b>E2E (cur.)</b>	12.5	0.325	0.00799
<b>E2E (nov.)</b>	19.4	0.315	0.00774
<b>E2E (rec.)</b>	19.3	0.292	0.00734
<b>Ours (cov.)</b>	20.2	<b>0.283</b>	<b>0.00734</b>
<b>Ours (sem.)</b>	<b>23.0</b>	0.319	0.00784
<b>Ours (obs.)</b>	22.5	0.305	0.00765
<b>Ours (view.)</b>	21.1	0.316	0.00769

**Table 5: Pose refinement performance:** optimizing camera viewpoints given a rendered target viewpoint.

Task	Metrics	Sim.	Mask R-CNN
<b>Rendering</b>	Per-class acc.	91.8	65.4
	mIoU	83.2	61.1
<b>Map comparison</b>	Sem acc.	99.8	99.7
	Sem prec.	36.2	14.1
	Sem rec.	29.8	8.5
<b>Planning</b>	ObjGoal Succ.	15.8	6.8
	ObjGoal SPL	15.3	6.5

**Table 6: NeRF semantic maps:** impact of the choice of ground-truth semantics vs. semantics estimated by Mask R-CNN when data is collected by *Ours (obs.)*.

is to autonomously collect data to build a NeRF model.

**Comparing trained policies** — Rewarding modular policies with obstacles (*Ours (obs.)*) and viewpoints (*Ours (view.)*) coverage appears to lead to the best overall performance when we consider the different metrics. Explored area coverage (*Ours (cov.)*) leads to highest *PointNav* performance, corroborating its importance for geometric tasks, whereas other semantic reward functions lead to higher *ObjectNav* performance, again corroborating its importance for semantic understanding of the scene.

**Semantics from Mask R-CNN** — Table 6 shows the impact of using Mask R-CNN to compute the semantics training data of the NeRF model vs semantics from simulation. As expected, performance drops because Mask R-CNN provides a much noisier training signal, which could partly be explained by the visual domain gap between the real world and simulators. However, performance on the different downstream tasks is still reasonable, showing that one could autonomously collect data and generate semantics training signal without requiring additional annotation.

#### 5.4. Qualitative results

**BEV maps** — Figure 7 gives examples of the BEV maps generated from the continuous representation: structural details and dense semantic information are nicely recovered (Left). Planned trajectories are close to the shortest paths, for both *PointGoal* tasks (Middle) and *ObjectGoal* (Right).

**Semantic rendering** — Figure 8 compares the segmenta-

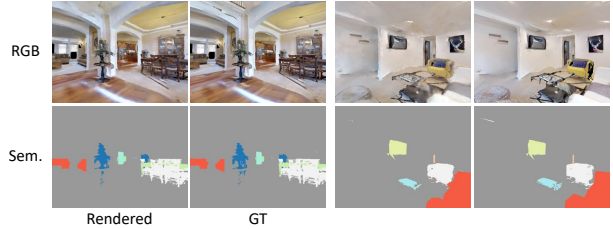


**Figure 8: Quality of semantic rendering** on pairs of images of different scenes, compared with GT from Sim. *Ours (obs.)*.

tion maps and RGB frames rendered with the continuous representation (trained with semantic masks from simulation) to the GT maps from the simulator. Again, the structure of the objects and even fine details are well recovered, and only very local noise is visible in certain areas. The semantic reconstruction is satisfying.

## 6. Conclusion

This work introduces a task involving navigating in a 3D environment to collect NeRF training data. We show that RL-trained modular policies outperform classic frontier-based exploration as well as other end-to-end RL baselines on this task, and compare different training reward functions. We also suggest evaluating NeRFs from a scene-understanding point of view and with robotics-oriented tasks: BEV map generation, planning, rendering, and camera pose refinement. Finally, we show that it is possible with the considered method to reconstruct house-scale scenes. Interesting future work could target fine-tuning navigation models automatically on a scene.

## References

- [1] Michal Adamkiewicz, Timothy Chen, Adam Caccavale, Rachel Gardner, Preston Culbertson, Jeannette Bohg, and Mac Schwager. Vision-only robot navigation in a neural radiance world. *RA-L*, 2022. 2
- [2] Peter Anderson, Angel X. Chang, Devendra Singh Chaplot, Alexey Dosovitskiy, Saurabh Gupta, Vladlen Koltun, Jana Kosecka, Jitendra Malik, Roozbeh Mottaghi, Manolis Savva, and Amir Roshan Zamir. On evaluation of embodied navigation agents. *arXiv preprint*, 2018. 6
- [3] Peter Anderson, Qi Wu, Damien Teney, Jake Bruce, Mark Johnson, Niko Sünderhauf, Ian Reid, Stephen Gould, and Anton Van Den Hengel. Vision-and-language navigation: Interpreting visually-grounded navigation instructions in real environments. In *CVPR*, 2018. 1
- [4] Devendra Singh Chaplot, Murtaza Dalal, Saurabh Gupta, Jitendra Malik, and Russ R Salakhutdinov. Seal: Self-supervised embodied active learning using exploration and 3d consistency. In *NeurIPS*, 2021. 1
- [5] Devendra Singh Chaplot, Dhiraj Gandhi, Abhinav Gupta, and Ruslan Salakhutdinov. Object goal navigation using

- goal-oriented semantic exploration. In *NeurIPS*, 2020. 1, 3, 4
- [6] Devendra Singh Chaplot, Dhiraj Gandhi, Saurabh Gupta, Abhinav Gupta, and Ruslan Salakhutdinov. Learning to explore using active neural slam. In *ICLR*, 2020. 1, 3, 4, 12
- [7] Devendra Singh Chaplot, Helen Jiang, Saurabh Gupta, and Abhinav Gupta. Semantic curiosity for active visual learning. In *ECCV*, 2020. 1, 12
- [8] Devendra Singh Chaplot, Ruslan Salakhutdinov, Abhinav Gupta, and Saurabh Gupta. Neural topological slam for visual navigation. In *CVPR*, 2020. 1
- [9] Tao Chen, Saurabh Gupta, and Abhinav Gupta. Learning exploration policies for navigation. In *ICLR*, 2019. 1, 3
- [10] Zhiqin Chen and Hao Zhang. Learning implicit fields for generative shape modeling. In *CVPR*, 2019. 2
- [11] Matt Deitke, Dhruv Batra, Yonatan Bisk, Tommaso Campari, Angel X Chang, Devendra Singh Chaplot, Changan Chen, Claudia Pérez D’Arpino, Kiana Ehsani, Ali Farhadi, et al. Retrospectives on the embodied ai workshop. *arXiv preprint*, 2022. 1
- [12] Christian Dornhege and Alexander Kleiner. A frontier-void-based approach for autonomous exploration in 3d. *Advanced Robotics*, 2013. 3
- [13] Haoqiang Fan, Hao Su, and Leonidas J Guibas. A point set generation network for 3d object reconstruction from a single image. In *CVPR*, 2017. 2
- [14] Stephan J Garbin, Marek Kowalski, Matthew Johnson, Jamie Shotton, and Julien Valentin. Fastnerf: High-fidelity neural rendering at 200fps. In *ICCV*, 2021. 2
- [15] Theophile Gervet, Soumith Chintala, Dhruv Batra, Jitendra Malik, and Devendra Singh Chaplot. Navigating to objects in the real world. *arXiv preprint*, 2022. 1
- [16] Thibault Groueix, Matthew Fisher, Vladimir G Kim, Bryan C Russell, and Mathieu Aubry. A papier-mâché approach to learning 3d surface generation. In *CVPR*, 2018. 2
- [17] Saurabh Gupta, James Davidson, Sergey Levine, Rahul Sukthankar, and Jitendra Malik. Cognitive mapping and planning for visual navigation. In *CVPR*, 2017. 1
- [18] Meera Hahn, Devendra Singh Chaplot, Shubham Tulsiani, Mustafa Mukadam, James M Rehg, and Abhinav Gupta. No rl, no simulation: Learning to navigate without navigating. In *NeurIPS*, 2021. 1
- [19] Kaiming He, Georgia Gkioxari, Piotr Dollár, and Ross Girshick. Mask R-CNN. In *ICCV*, 2017. 3, 5
- [20] Dirk Holz, Nicola Basilico, Francesco Amigoni, and Sven Behnke. Evaluating the efficiency of frontier-based exploration strategies. In *ISR*, 2010. 3
- [21] Jacob Krantz, Erik Wijmans, Arjun Majumdar, Dhruv Batra, and Stefan Lee. Beyond the nav-graph: Vision-and-language navigation in continuous environments. In *ECCV*, 2020. 1
- [22] Tsung-Yi Lin, Michael Maire, Serge Belongie, James Hays, Pietro Perona, Deva Ramanan, Piotr Dollár, and C Lawrence Zitnick. Microsoft coco: Common objects in context. In *ECCV*, 2014. 6
- [23] William E Lorensen and Harvey E Cline. Marching cubes: A high resolution 3d surface construction algorithm. *ACM siggraph computer graphics*, 1987. 14
- [24] Eric Marchand. Direct visual servoing in the frequency domain. *RA-L*, 2020. 6
- [25] Pierre Marza, Laetitia Matignon, Olivier Simonin, and Christian Wolf. Multi-object navigation with dynamically learned neural implicit representations. *arXiv preprint arXiv:2210.05129*, 2022. 2
- [26] Pierre Marza, Laetitia Matignon, Olivier Simonin, and Christian Wolf. Teaching agents how to map: Spatial reasoning for multi-object navigation. In *IROS*, 2022. 1
- [27] Daniel Maturana and Sebastian Scherer. Voxnet: A 3d convolutional neural network for real-time object recognition. In *IROS*, 2015. 2
- [28] Lars Mescheder, Michael Oechsle, Michael Niemeyer, Sebastian Nowozin, and Andreas Geiger. Occupancy networks: Learning 3d reconstruction in function space. In *CVPR*, 2019. 2
- [29] Lina Mezghan, Sainbayar Sukhbaatar, Thibaut Lavril, Oleksandr Maksymets, Dhruv Batra, Piotr Bojanowski, and Kartheek Alahari. Memory-augmented reinforcement learning for image-goal navigation. In *IROS*, 2022. 1
- [30] Ben Mildenhall, Pratul P Srinivasan, Matthew Tancik, Jonathan T Barron, Ravi Ramamoorthi, and Ren Ng. Nerf: Representing scenes as neural radiance fields for view synthesis. In *ECCV*, 2020. 2, 3
- [31] So Yeon Min, Devendra Singh Chaplot, Pradeep Ravikumar, Yonatan Bisk, and Ruslan Salakhutdinov. Film: Following instructions in language with modular methods. In *ICLR*, 2022. 1
- [32] Thomas Müller, Alex Evans, Christoph Schied, and Alexander Keller. Instant neural graphics primitives with a multiresolution hash encoding. 2022. 2, 12
- [33] Xuran Pan, Zihang Lai, Shiji Song, and Gao Huang. Activenerf: Learning where to see with uncertainty estimation. In *ECCV*, 2022. 3
- [34] Jeong Joon Park, Peter Florence, Julian Straub, Richard Newcombe, and Steven Lovegrove. DeepSDF: Learning continuous signed distance functions for shape representation. In *CVPR*, 2019. 2
- [35] Santhosh K. Ramakrishnan, Devendra Singh Chaplot, Ziad Al-Halah, Jitendra Malik, and Kristen Grauman. Poni: Potential functions for objectgoal navigation with interaction-free learning. In *CVPR*, 2022. 1
- [36] Santhosh K Ramakrishnan, Dinesh Jayaraman, and Kristen Grauman. An exploration of embodied visual exploration. *IJCV*, 2021. 7, 8
- [37] Ram Ramrakhya, Eric Undersander, Dhruv Batra, and Abhishek Das. Habitat-web: Learning embodied object-search strategies from human demonstrations at scale. In *CVPR*, 2022. 1
- [38] Nikolay Savinov, Anton Raichuk, Damien Vincent, Raphael Marinier, Marc Pollefeys, Timothy Lillicrap, and Sylvain Gelly. Episodic curiosity through reachability. In *ICLR*, 2018. 1, 3
- [39] Manolis Savva, Abhishek Kadian, Oleksandr Maksymets, Yili Zhao, Erik Wijmans, Bhavana Jain, Julian Straub, Jia Liu, Vladlen Koltun, Jitendra Malik, Devi Parikh, and Dhruv Batra. Habitat: A platform for embodied ai research. In *ICCV*, 2019. 5

- [40] John Schulman, Filip Wolski, Prafulla Dhariwal, Alec Radford, and Oleg Klimov. Proximal policy optimization algorithms. *arXiv preprint*, 2017. 3
- [41] James A Sethian. A fast marching level set method for monotonically advancing fronts. 1996. 3
- [42] Karen Simonyan and Andrew Zisserman. Very deep convolutional networks for large-scale image recognition. *arXiv preprint*, 2014. 6
- [43] Edgar Sucar, Shikun Liu, Joseph Ortiz, and Andrew J Davison. imap: Implicit mapping and positioning in real-time. In *ICCV*, 2021. 2
- [44] Andrew Szot, Alex Clegg, Eric Undersander, Erik Wijmans, Yili Zhao, John Turner, Noah Maestre, Mustafa Mukadam, Devendra Chaplot, Oleksandr Maksymets, Aaron Gokaslan, Vladimir Vondrus, Sameer Dharur, Franziska Meier, Wojciech Galuba, Angel Chang, Zsolt Kira, Vladlen Koltun, Jitendra Malik, Manolis Savva, and Dhruv Batra. Habitat 2.0: Training home assistants to rearrange their habitat. In *NeurIPS*, 2021. 5
- [45] Matthew Tancik, Vincent Casser, Xinchun Yan, Sabeek Pradhan, Ben Mildenhall, Pratul P Srinivasan, Jonathan T Barron, and Henrik Kretzschmar. Block-nerf: Scalable large scene neural view synthesis. In *CVPR*, 2022. 2
- [46] Matthew Tancik, Ethan Weber, Evonne Ng, Ruilong Li, Brent Yi, Justin Kerr, Terrance Wang, Alexander Kristoffersen, Jake Austin, Kamyar Salahi, et al. Nerfstudio: A modular framework for neural radiance field development. *arXiv preprint*, 2023. 3, 7
- [47] Suhani Vora, Noha Radwan, Klaus Greff, Henning Meyer, Kyle Genova, Mehdi SM Sajjadi, Etienne Pot, Andrea Tagliasacchi, and Daniel Duckworth. Nesf: Neural semantic fields for generalizable semantic segmentation of 3d scenes. *arXiv preprint*, 2021. 2
- [48] Fei Xia, Amir R Zamir, Zhiyang He, Alexander Sax, Jitendra Malik, and Silvio Savarese. Gibson env: Real-world perception for embodied agents. In *CVPR*, 2018. 6
- [49] Yiheng Xie, Towaki Takikawa, Shunsuke Saito, Or Litany, Shiqin Yan, Numair Khan, Federico Tombari, James Tompkin, Vincent Sitzmann, and Srinath Sridhar. Neural fields in visual computing and beyond. *arXiv preprint*, 2021. 2
- [50] Kai Xu, Lintao Zheng, Zihao Yan, Guohang Yan, Eugene Zhang, Matthias Niessner, Oliver Deussen, Daniel Cohen-Or, and Hui Huang. Autonomous reconstruction of unknown indoor scenes guided by time-varying tensor fields. 2017. 3
- [51] Brian Yamauchi. A frontier-based approach for autonomous exploration. In *CIRA*, 1997. 3
- [52] Lin Yen-Chen, Pete Florence, Jonathan T Barron, Alberto Rodriguez, Phillip Isola, and Tsung-Yi Lin. inerf: Inverting neural radiance fields for pose estimation. In *IROS*, 2021. 2, 6, 14
- [53] Alex Yu, Vickie Ye, Matthew Tancik, and Angjoo Kanazawa. pixelnerf: Neural radiance fields from one or few images. In *CVPR*, 2021. 2
- [54] Huangying Zhan, Jiyang Zheng, Yi Xu, Ian Reid, and Hamid Rezaatoughi. Activermap: Radiance field for active mapping and planning. 2022. 3
- [55] Richard Zhang, Phillip Isola, Alexei A Efros, Eli Shechtman, and Oliver Wang. The unreasonable effectiveness of deep features as a perceptual metric. In *CVPR*, 2018. 5
- [56] Shuaifeng Zhi, Tristan Laidlow, Stefan Leutenegger, and Andrew J Davison. In-place scene labelling and understanding with implicit scene representation. In *ICCV*, 2021. 2, 3, 5, 7
- [57] Shuaifeng Zhi, Edgar Sucar, Andre Mouton, Iain Haughton, Tristan Laidlow, and Andrew J Davison. ilabel: Interactive neural scene labelling. *arXiv preprint*, 2021. 2
- [58] Yuke Zhu, Roozbeh Mottaghi, Eric Kolve, Joseph J Lim, Abhinav Gupta, Li Fei-Fei, and Ali Farhadi. Target-driven visual navigation in indoor scenes using deep reinforcement learning. In *ICRA*, 2017. 1
- [59] Zihan Zhu, Songyou Peng, Viktor Larsson, Zhaopeng Cui, Martin R Oswald, Andreas Geiger, and Marc Pollefeys. Nicer-slam: Neural implicit scene encoding for rgb slam. *arXiv preprint*, 2023. 2
- [60] Zihan Zhu, Songyou Peng, Viktor Larsson, Weiwei Xu, Hujun Bao, Zhaopeng Cui, Martin R Oswald, and Marc Pollefeys. Nice-slam: Neural implicit scalable encoding for slam. *CVPR*, 2022. 2

## Appendix

### A. Study of correlations between rewards and downstream tasks performance

We analyze the correlation between cumulated reward, used as a metric, and NeRF evaluation metrics. For each reward definition, we compute cumulated reward (*cov.*, *sem.*, *obs.*, *view.*) after 1500 timesteps. 5 runs for each policy on each scene provide 20 data points for each reward function on each scene. In Table 7 we report the Pearson correlation coefficient between the reward function and NeRF evaluation metric for the 5 Gibson val scenes if the associated p-value is lower than 5%, otherwise “-”. As can be seen, obstacle coverage is the most correlated to NeRF evaluation, followed by viewpoints coverage.

### B. Navigating with sensor and actuation noise

All experiments in this work were conducted following task specifications in [7], among which are perfect odometry information and actuation. We thus conduct an additional experiment to evaluate the impact of sensor and actuation noise on AutoNeRF. We add noise using realistic models from [6] and correct odometry information using the pose estimation module trained in [6]. This allows our modular policy (*Ours (obs.)*) to explore properly environments and collect NeRF training data. We then refine camera poses with bundle adjustment before using them to train NeRF models. Tables 8, 9, 10, 11 show that performance obviously decreases when adding noise, but we still reach a satisfying performance in all metrics. It is also important to note that, even after using the pose estimation module and post-processing bundle adjustment, camera poses spanning such large scenes are still noisy, and training NeRF models on noisy poses is considered a challenging problem in the literature. Better performance might thus come from new techniques to make NeRF models more robust to camera pose noise, which is orthogonal to the contribution in this work.

### C. Generalization to another NeRF variant

To show that AutoNeRF can be generalized to another NeRF variant, we train an *Instant-NGP* [32] model on data collected by the modular policy (*Ours (obs.)*) and compare its rendering performance with the one of *Semantic Nerfacto* in Table 12. As can be seen, rendering performance is close.

### D. Navigating inside a NeRF-generated mesh

To further evaluate the quality of the geometry learnt by an autonomously generated NeRF and assess to what extent it

can be used inside a simulator, we perform PointGoal navigation on an original mesh and a NeRF-generated one for 4 Gibson val scenes. The considered agent is based on the modular policy introduced in the main paper, restricted to the planning part: the output of the Global Policy is replaced with the input PointGoal vector. Planning is performed using the Fast Marching Method, relying on the map channels storing information about obstacles and explored area. Table 13 shows that there is a performance drop between the navigating on the original Gibson meshes and the reconstructed ones, but Success and SPL are close. The performance on the original mesh is a “soft upper bound”, as data was collected from navigating in this original mesh, before training a NeRF and finally generating a new mesh representation. These results show that our NeRF-generated mesh features a satisfying geometry, allowing to navigate properly when loaded within the Habitat simulator. Some further mesh post-processing could be needed, along with additional work on improving lighting within the simulator.

### E. Details on downstream tasks

**Metric Map Estimation** — Cells in the occupancy and semantic top-down maps generated from NeRF models are of size  $1cm \times 1cm$ . In order to create the occupancy map, we first compute a 3D voxel grid by regularly querying the NeRF density head between scene bounds along  $x$  and  $z$  axes, and between 0 and the agent’s height along the vertical  $y$  axis. We then transform the 3D grid into a 2D top-down map by applying a sum operation along the vertical axis. We found that, when using a *Semantic Nerfacto* model, generating a point cloud where each point is associated with a semantics class from the train camera poses works best when generating the semantics top-down map. The point cloud is converted into a 3D voxel grid, where each cell is associated with a channel for each semantics class. A per-class sum operation can finally transform the 3D grid into a 2D map with one channel per class. The same cell resolution is used when generating ground-truth maps from the Habitat simulator.

**Planning** — Resolution of the top-down maps used to plan a path are the same as for the *Metric Map Estimation* task. Once generated, the path is evaluated on the ground-truth top-down map from the Habitat simulator. In order to account for the size of a potential robot of radius  $18cm$ , obstacles on the ground-truth map are dilated. We also apply a dilation with a  $20cm$  radius to obstacles on our top-down map before planning the path.

For a given episode  $i$ , *Success*  $S_i$  is 1 if the last cell in the planned path is closer than 1m to the goal and if less than 10 planned cells are obstacles, otherwise it is 0. We chose to allow up to 10 obstacle cells on the planned path to keep the task from being overly complex and thus uninformative.

Reward	PSNR (RGB rendering)					Per-class acc (Sem rendering)					Occ. recall (Map comp.)					Sem. recall (Map comp.)				
	0	1	2	3	4	0	1	2	3	4	0	1	2	3	4	0	1	2	3	4
cov.	0.73	0.77	0.95	0.48	—	—	0.59	<b>0.97</b>	0.60	—	0.50	0.75	<b>0.94</b>	0.47	—	—	0.47	<b>0.93</b>	—	—
sem.	0.52	—	0.84	0.62	—	—	0.66	0.82	0.61	—	0.53	0.60	0.80	0.48	0.46	—	<b>0.73</b>	0.72	—	—
obs.	<b>0.88</b>	<b>0.83</b>	<b>0.96</b>	<b>0.70</b>	—	<b>0.48</b>	<b>0.79</b>	0.95	<b>0.76</b>	0.48	<b>0.73</b>	<b>0.87</b>	<b>0.94</b>	<b>0.56</b>	0.64	—	0.72	0.91	—	—
view.	0.83	0.55	0.93	0.67	<b>0.55</b>	—	0.48	0.87	0.70	<b>0.55</b>	0.66	—	0.88	0.53	<b>0.69</b>	—	0.60	0.80	—	—
Reward	PointGoal Succ (Planning)					ObjectGoal Succ (Planning)					Rot. conv. rate (Pose Ref.)					Trans. conv. rate (Pose Ref.)				
	0	1	2	3	4	0	1	2	3	4	0	1	2	3	4	0	1	2	3	4
cov.	—	—	0.63	—	—	—	—	0.62	—	—	0.49	—	0.69	—	—	0.54	—	0.72	—	—
sem.	—	—	—	—	—	—	—	0.44	—	—	0.67	—	0.70	—	—	0.52	—	0.73	<b>0.63</b>	0.49
obs.	—	—	<b>0.66</b>	—	—	—	—	<b>0.66</b>	—	—	0.69	—	0.72	—	0.59	0.66	—	0.75	0.52	0.65
view.	—	—	0.60	—	<b>0.53</b>	—	—	0.60	—	<b>0.53</b>	<b>0.74</b>	—	<b>0.75</b>	—	<b>0.66</b>	<b>0.70</b>	—	<b>0.78</b>	0.60	<b>0.81</b>

**Table 7: Correlations between reward metrics and selected NeRF evaluation metrics.** Pearson correlation coefficients are reported if the associated p-value is lower than 5%, otherwise —. Columns denoted 0, 1, 2, 3, 4 correspond to the 5 Gibson val scenes. Obstacle coverage is the most correlated to NeRF evaluation metrics, followed by viewpoints coverage.



**Figure 9: Quality of semantic rendering** on pairs of images of different scenes, compared with GT from Sim. NeRF training data is collected by *Ours (obs)*.

Policy	RGB				Semantics	
	Noise	PSNR ↑	SSIM ↑	LPIPS ↓	Per-class acc ↑	mIoU ↑
<b>Ours (obs.)</b>	—	25.56	0.846	0.203	91.8	83.2
<b>Ours (obs.)</b>	✓	20.87	0.761	0.264	85.4	73.6

**Table 8: Rendering performance with sensor and actuation noise** on uniformed sampled viewpoints of the full scene after training on a single trajectory. NeRF training data is collected by *Ours (obs)*.

Policy	Occupancy				Semantics		
	Noise	Acc. ↑	Prec. ↑	Rec. ↑	Acc ↑	Prec. ↑	Rec. ↑
<b>Ours (obs.)</b>	—	86.4	89.4	76.5	99.8	36.2	29.8
<b>Ours (obs.)</b>	✓	86.8	89.8	69.6	99.7	29.9	24.1

**Table 9: Map estimation performance with sensor and actuation noise:** comparison of BEV maps estimated from the NeRF. NeRF training data is collected by *Ours (obs)*.

For both *PointGoal planning* and *ObjectGoal planning*, we report mean *Success* and *SPL* over a total of  $N$  planning episodes. Mean *Success* is  $\frac{1}{N} \sum_{i=1}^N S_i$ . Mean *SPL* takes

Policy	PointGoal		ObjectGoal		
	Noise	Succ. ↑	SPL ↑	Succ. ↑	SPL ↑
<b>Ours (obs.)</b>	—	38.2	37.8	15.8	15.3
<b>Ours (obs.)</b>	✓	34.5	33.8	12.9	12.4

**Table 10: Planning performance with sensor and actuation noise** on the BEV maps estimated from the NeRF obtained with the *Fast Marching* method. NeRF training data is collected by *Ours (obs)*.

Policy	Noise	Conv. rate ↑	Rot. Error (°) ↓	Trans. Error (m) ↓
<b>Ours (obs.)</b>	—	22.5	0.305	0.00765
<b>Ours (obs.)</b>	✓	7.9	0.405	0.01125

**Table 11: Pose refinement performance with sensor and actuation noise:** optimizing camera viewpoints given a rendered target viewpoint. NeRF training data is collected by *Ours (obs)*.

into account both success and path efficiency to reach the goal and is equal to  $\frac{1}{N} \sum_{i=1}^N S_i \frac{\ell_i}{\max(p_i, \ell_i)}$ , where  $\ell_i$  is the shortest path distance from the start point to the goal and  $p_i$  is the length of the planned path.



**Figure 10: BEV map tasks:** Generation of semantic BEV maps (Left), *PointGoal* (Middle) and *ObjectGoal* planning (Right). NeRF training data is collected by *Ours (obs)*.

NeRF model	PSNR $\uparrow$	SSIM $\uparrow$	LPIPS $\downarrow$
<b>Semantic Nerfacto</b>	25.56	0.846	0.203
<b>Instant-NGP</b>	24.92	0.806	0.279

**Table 12: Generalizing to another NeRF variant:** Rendering performance of an Instant-NGP model trained on data collected by *Ours (obs)*.

Mesh	Success $\uparrow$	SPL $\uparrow$
<b>Original Gibson mesh</b>	88.1	73.3
<b>Rollout <math>\rightarrow</math> NeRF training <math>\rightarrow</math> Mesh generation</b>	78.4	67.7

**Table 13: Navigating inside a NeRF-generated mesh:** Average *PointGoal* performance of a policy planning a path to the goal with the Fast Marching Method and taking discrete actions on 4 Gibson val scenes in the Habitat simulator, from either the original mesh (**Gibson**) or the mesh extracted from the NeRF model (**Rollout + NeRF train. + Mesh gen.**) trained from autonomously collected data by *Ours (obs)*. Our reconstruction does not require depth data.

**Pose Refinement** — At each pose refinement optimization step, we would ideally want to render the full image associated with the estimated camera pose to compare with the RGB frame from the camera. As already noticed in previous work [52], doing this is expensive, and we thus instead randomly sample pixels to be rendered within the image at each optimization step.

**Mesh generation** — In order to create a mesh from a trained NeRF model, we first build a 3D voxel grid by

querying the implicit representation regularly on a grid between the scene bounds. Each voxel will be associated with a density, and either a color or a semantics class depending on the nature of the mesh to generate. The voxel grid is converted into a mesh by applying the Marching Cubes algorithm [23].

## F. Qualitative examples

We provide additional qualitative results for the rendering, map estimation, planning, pose refinement and mesh generation tasks.

**Rendering** — Figure 9 shows additional rendering examples from a *Semantic Nerfacto* model trained on data collected by the modular policy, *Ours(obs)*, with semantics ground-truth from the Habitat simulator. Both RGB and semantics rendering are accurate for camera poses that were not seen during NeRF training.

**Metric Map Estimation and Planning** — Figure 10 shows additional results regarding semantic top-down map generation and path planning (both *PointGoal* and *ObjectGoal*) from a *Semantic Nerfacto* model trained on data collected by the modular policy, *Ours(obs)*, with semantics ground-truth from the Habitat simulator. As done in Figure 7 in the main paper, we present qualitative results from a *Semantic Nerfacto* model as it is the one we use in quantitative results (Tables 2, 3, 4, 5 in the main paper). Higher-quality geometry could be obtained from a vanilla *Semantic NeRF* model,

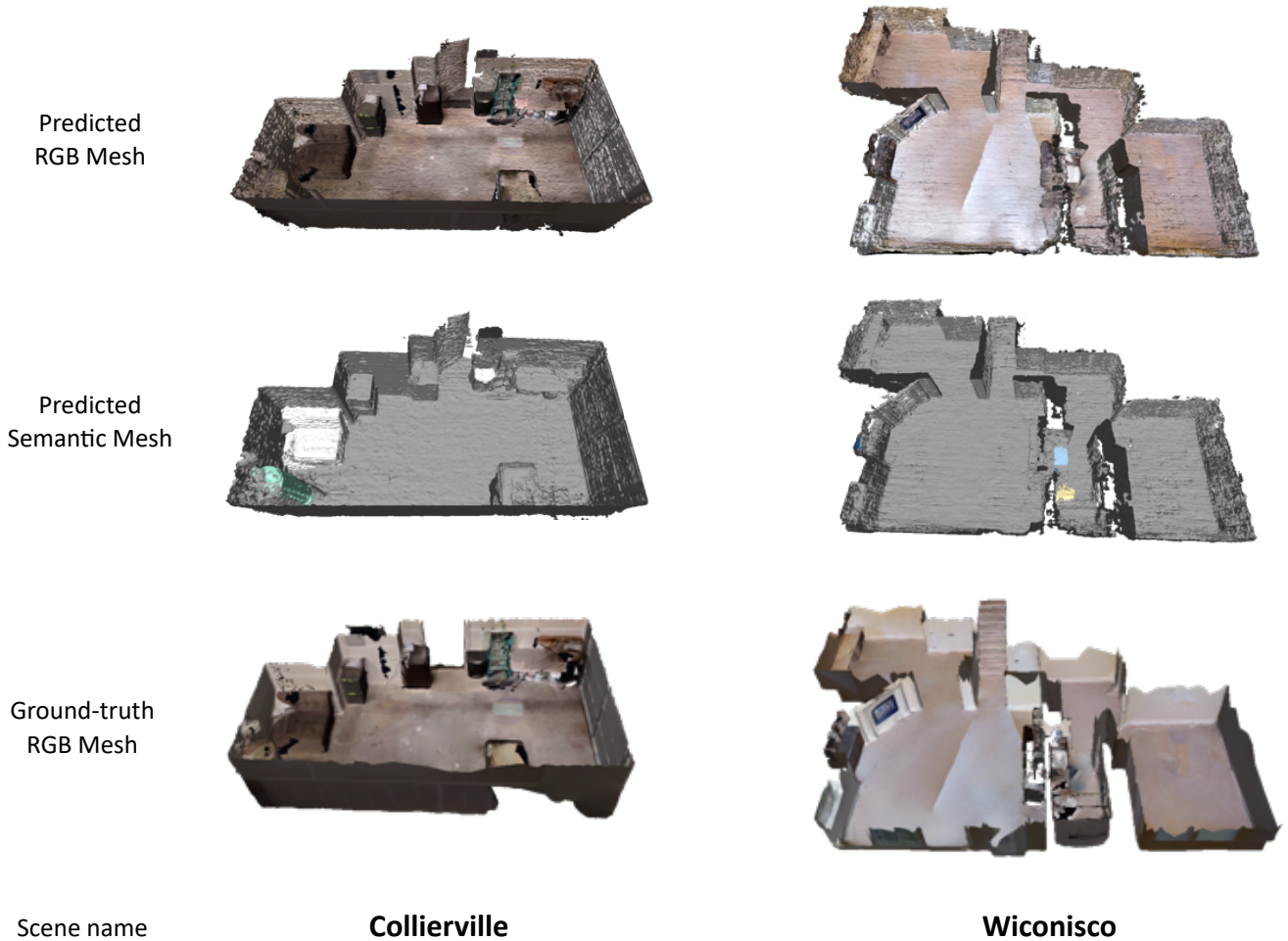


**Figure 11: Mesh reconstruction:** reconstruction of 2 Gibson val scenes extracted from a NeRF model trained on data gathered by our *Ours (obs)* modular policy. Both geometry, semantics, and appearance are satisfying.

but with the cost of significantly longer training time. Semantic objects are properly localized, geometry is correct, except for some room corners that are more challenging to properly reconstruct with the fast-trained *Semantic Nerfacto*. Paths can be planned to both end points specified as positions on the grid and to the closest object of a given category.

**Pose refinement** — Camera pose optimization results are best viewed as videos. Examples are available on the [project page](#), showcasing the evolution of *Semantic Nerfacto* rendered frame compared with the ground-truth camera view during the optimization process. The NeRF was trained on data collected by the modular policy, *Ours(obs)*.

**Mesh Generation** — Figure 11 shows the RGB and semantics meshes extracted from a *vanilla Semantic NeRF* model trained on data collected by the modular policy, *Ours(obs)*, with semantics ground-truth from the Habitat simulator. The RGB mesh is close to the ground-truth original Gibson

mesh, while being built without any depth input. Objects of interest are properly segmented on the semantics mesh.